Article

Evaluating the targeting efficiency of anti-EGFR functionalised nanoparticles to Head and Neck cancer cells for use in NIR-II optical window

Teklu Egnuni[1], Nicola Ingram[1], P. Louise Coletta[1] and James R. McLaughlan[1,2*]

[1]Leeds Institute of Medical Research, University of Leeds, St. James's University Hospital, Leeds, LS9 7TF, UK; T.Egnuni@leeds.ac.uk (T.E); N.Ingram@leeds.ac.uk (N.I) and P.L>Coletta@leeds.ac.uk (P.L.C)
[2]School of Electronic and Electrical Engineering, University of Leeds, LS2 9JT, UK; J.R>McLaughlan@leeds.ac.uk (J.M)
*Correspondence: e-mail: J.R.McLaughlan@leeds.ac.uk; Tel: +44(0) 113 343 0956

***Abstract**:* Gold nanoparticles have been indicated for use in a diagnostic and/or therapeutic role in several cancer types. The use of gold nanorods (AuNRs) with a surface plasmon resonance (SPR) in the second Near-Infrared II (NIR-II) optical window promises deeper anatomical penetration through increased maximum permissible exposure and lower optical attenuation. In this study, the targeting efficiency of anti-epidermal growth factor receptor (EGFR) antibody functionalised AuNRs with an SPR at 1064 nm was evaluated *in vitro*. Four cell lines, KYSE-30, CAL-27, Hep-G2 and MCF-7 that either over or under expressed EGFR were used. This expression was confirmed by flow cytometry and immunofluorescence. Cytotoxicity assays showed no AuNRs toxicity to both EGFR positive and EGFR negative cell lines up to a concentrations of 19 µg/ml. Optical microscopy demonstrated a significant difference ($p<0.0001$) between targeted AuNRs (tAuNRs) and untargeted AuNRs (uAuNRs) in all four cancer cell lines. This study demonstrates that anti-EGFR functionalisation significantly increased the number of tAuNRs associated with each EGFR positive cancer cell. This successful targeting highlights the use of tAuNRs for molecular photoacoustic imaging or tumour treatment through plasmonic photothermal therapy.

Key Words: Gold nanorods; Targeted; EGFR; HNSCC; Uptake; and NIR-II window

---

1. Introduction

A variety of nanoparticles such as proteins, metals, carbons, lipids, viral amongst others are widely used as contrast agents in cancer theranostics research today [1]. Due to their stability and biocompatibility, strong optical absorbance through SPR properties, and suitability for surface functionalisation, gold nanoparticles of various size and shape have potential for widespread use in the detection and treatment of cancers [2, 3]. Gold nanoparticles can be manufactured with a wide range of absorption spectrum commonly classified as NIR-I and NIR-II with 650 - 900 nm and 1000 - 1200 nm wavelengths, respectively [4, 5]. It is suggested that particles with an SPR in the NIR-II optical window have a deeper tissue penetration and better sensitivity for early detection of tumour cells than those within NIR-I wavelength and visible light regions [6-8]. Nanoparticles can act as contrast agents for photoacoustic imaging (PAI), and pre-clinical studies show their use in the diagnosis of early stage cancers [9, 10]. Photothermal therapy (PTT) is an emerging therapeutic technique whereby nanomaterials absorb light in the near-infrared (NIR) window and convert it to heat in order to selectively ablate cancerous tissues thermally [11, 12].

Head and neck squamous cell carcinoma (HNSCC) is one of the most common cancers worldwide and contributes to 90% of all head and neck cancers [13]. Alcohol, tobacco and human papilloma virus (HPV) infection are major known risk factors of HNSCC [14]. Although the current standard of therapy for HNSCC patients has an overall 5-year survival rate of 35 - 54% [15], these conventional therapies suffer from debilitating side effects such as temporary or permanent loss of

Preprints (www.preprints.org) | NOT PEER-REVIEWED | Posted: 29 March 2021 doi:10.20944/preprints202103.0687.v1

speech, loss of hearing, chewing and/or swallowing, fatigue, hair loss, sore throat following damage to healthy tissues of the throat, salivary gland, thyroid gland and lymph nodes [16-19]. The overall patient survival also depends on the stage and molecular subtypes of the HNSCC. Chung *et al [20]* and Walter *et al* [21] identified four different molecular subtypes of HNSCC with different degrees of recurrence-free-survival using gene expression techniques and showed that the subtype with high expression of epidermal growth factor receptor (EGFR) had the worse outcome.

Despite their potential for increased tissue penetration for imaging and/or therapy, there is little understanding of the long term toxicity, biocompatibility and tissue clearance of 1064 nm SPR AuNRs [22]. To date, cancer targeted therapy using PTT remains an unmet challenge and there is a paucity of research conducted using AuNRs in the NIR-II window. Therefore, we compared the specific targeting potential of cetuximab (anti-EGFR antibody) functionalised AuNRs in both EGFR positive and negative cancer cell lines with a view to their future utility in PTT for treatment of aggressive HNSCC.

2. Materials and Methods

2.1. Cell culture

CAL-27 (ATCC CRL-2095) and MCF-7 (ATCC HTB-22) were cultured in DMEM (#31966-021, Gibco) with 10% (v/v) FBS (#F7524, Sigma). KSYE-30, was grown in a 1:1 ratio of RPMI 1640 (#61870, Gibco) and Ham's F12 (#31765-027, Gibco) supplemented with 2 mM Glutamine (#25030-081, Gibco) and 2% (v/v) FBS. Hep G2 cells (ATCC HB-8065) were cultured in RPMI 1640 (#61870, Gibco) with 10% (v/v) FBS. All cells were passaged when 70-80% confluent and incubated at 37 °C in a humidified incubator under 5% CO_2.

2.2. Flow Cytometry

Cell suspensions were incubated for 2 hrs at 37 °C to allow for receptor recycling following trypsinisation and then centrifuged at 400g for 5 minutes. $1x10^6$ cells in 100 µl FACS buffer (10% FBS in PBS) were blocked with 5 µl Human TruStain FcX (#422301, Biolegend) for 10 minutes on ice. The cells were then incubated with either 0.05 µg recombinant monoclonal human EGFR (Research Grade Cetuximab Biosimilar, #FAB9577B, R&D Systems) or mouse IgG1 isotype (#IC002B, R&D Systems) biotinylated antibodies for 30 minutes on ice. Following washing, streptavidin-FITC secondary antibody (#F0030, R&D systems) was added at a concentration of 10 µl/10^6 cells (10 µg/ml) and incubated with the cells for 30 minutes on ice in the dark place. Cells were washed and then analysed on an Attune Flow Cytometer (Applied Biosystems) and the results were analysed using the Attune software (Applied Biosystems, Life Technologies). The percentage of EGFR positive cells, mean and median fluorescent intensities were determined for all the four cancer cell types stained using anti-EGFR antibody compared to the isotype control.

2.3. *Immunofluorescence imaging (IF).*

Cells were plated onto glass coverslips and allowed to grow to 70% confluence. Cells were washed with PBS and fixed in 4% PFA for 10 minutes at RT. The wells were further washed twice in PBS for 5 minutes each time and blocked in 10% (v/v) FBS for 1 hour. Cells were then incubated with 1 µg/ml of primary anti-human EGFR goat polyclonal antibody (#AF231, R&D Systems) or a biotinylated anti-human IgG1 rabbit monoclonal antibody (#31-1019-02, 2BScientific Limited) as a control in a humidified chamber for 1 hr at RT. FITC Rabbit anti-goat secondary antibody (#31509, Invitrogen) or streptavidin-FITC was added following 3 washes of 5 minutes each in PBS and counterstained using a Prolong Gold Antifade Mount nuclear stain (#P36930, ThermoFisher Scientific). The stained cells were imaged using Zeiss microscope using filters for DAPI, (acquisition time, 20 ms) and FITC (175 ms).

Preprints (www.preprints.org) | NOT PEER-REVIEWED | Posted: 29 March 2021 doi:10.20944/preprints202103.0687.v1

2.4. Gold nanorods (AuNRs)

Neutravidin coated 10 nm x 67 nm gold nanorods (#C12-10-1064-TN-PBS-50-1) with a 6.7 aspect ratio (AR) were purchased from Nanopartz (Loveland, CO, USA). The AuNRs had a localised longitudinal and transverse surface plasmon resonance (SPR) and at 1064 and 506 nm, respectively. The concentration of EGFR-targeted and untargeted AuNRs was determined using Genesys20 Ultraviolet–visible-NIR spectroscopy (UV-Vis-NIR) (#4001-0, ThermoFisher Scientific) analysis based on OD-ml according to the manufacturer's recommendation. For the untargeted group, 2 µl of the stock solution was diluted in 198 µl of PBS in a sterile Eppendorf tube (E1415-1510, Star Lab) following 5 minutes sonication in an unheated water bath and 30 seconds vigorous vortexing of the stock AuNRs. The diluted AuNRs were transferred into micro quartz cuvette tubes (CV10Q700, Thorlabs) and the absorbance values of AuNRs were measured following baseline determination using a blank sample (PBS) using Jenway visible spectrophotometry software according to the manufacturer's protocol.

Similarly, the UV-vis absorbance values of targeted AuNRs were also determined after 2 µl of AuNRs were allowed to conjugate with 5.6 µl of biotinylated anti-EGFR (10 µg/ml) antibody in PBS by vortexing at 1000 RPM for 2 hrs at RT. This conjugation process of neutravidin coated AuNRs and biotinylated antibody resulted in the formation of tAuNR conjugate (Figure 1A). The concentration of the AuNRs samples was calculated from the peak UV-Vis-NIR absorbance values at 1064 nm after correcting for the dilution factor and subtracting the absorbance values of the blank sample [23]. Quantitation of targeted and untargeted AuNRs was repeated three times. All absorbance values at different wavelengths were divided by the maximum absorbance unit at 400 nm wavelength in order to get extinction values [24] and the UV-Vis analysis graph was plotted using normalised extinction (a.u.) and wavelength (nm). Compared to the uAuNRs the absorbance values of tAuNRs UV-Vis were significantly lower and this could be due to the antibody AuNRs conjugation process involving 3 consecutive washes in PBS. Overall, a loss of 64.1%, 45.7% and 23.2%, were calculated during 3 different time periods and an average total loss of 44.3% AuNRs was calculated following antibody conjugation process and this loss was added as a compensation onto all targeted groups. Figure 1B shows the normalised extinction values of both uAuNR and tAuNR at different wavelengths following three repeat measurements using UV-Vis.

Preprints (www.preprints.org) | NOT PEER-REVIEWED | Posted: 29 March 2021 doi:10.20944/preprints202103.0687.v1

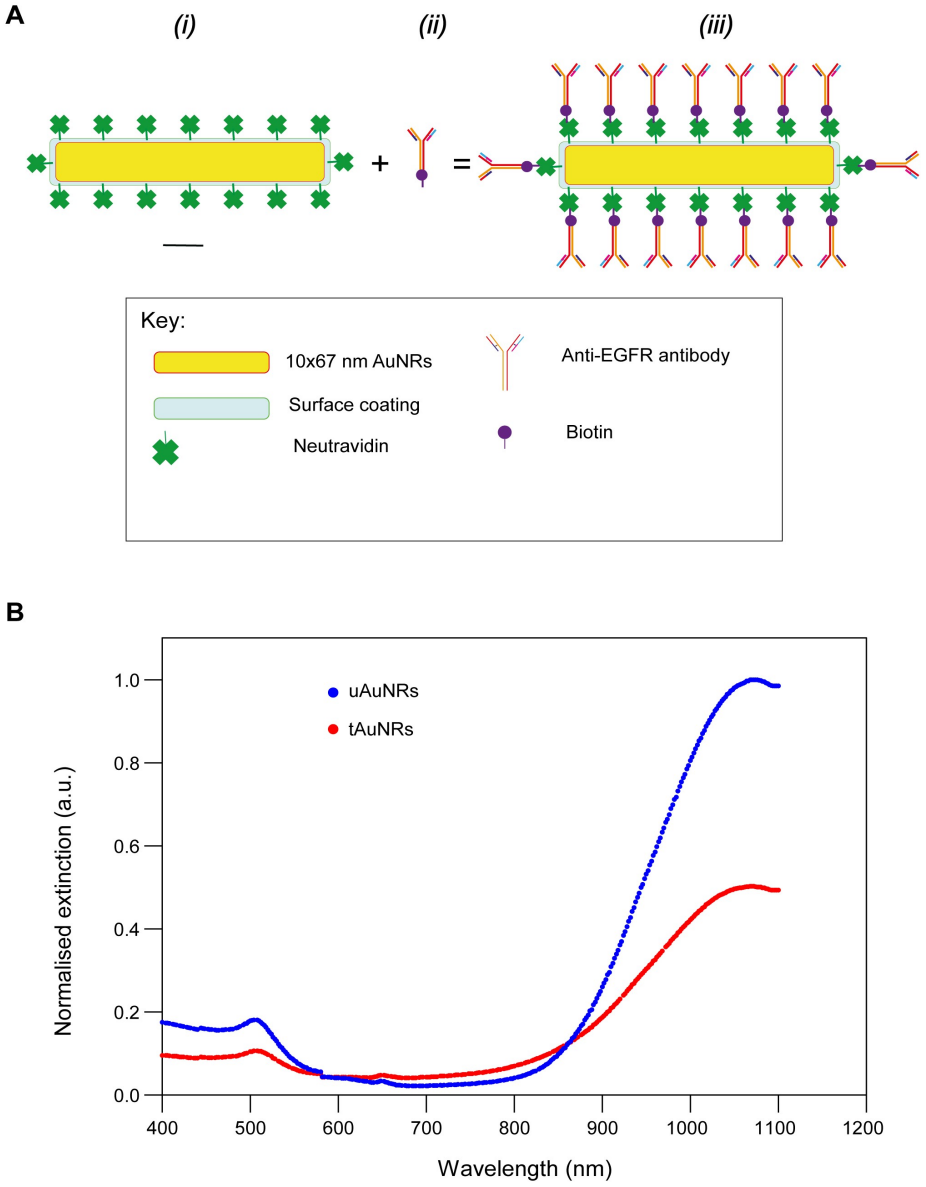

Figure 1. Antibody conjugation process reduced the number of AuNRs. (**A**) Schematic diagram showing a structure of tAuNRs. Neutravidin (4 x 5 x 5.6 nm) coated, 10 nm x 67 nm AuNRs (*i*) were added to biotinylated (5.2 nm x 5.2 nm) Anti-EGFR antibody (*ii*) in a 1:2.8 ratio (v/v) and conjugated to form tAuNRs (*iii*). Scale bar, 10 nm. (**B**) Absorbance measurement was used to plot the normalised extinction values of targeted and untargeted AuNRs. A loss of 44.3% ±20.5of AuNRs from the conjugation process was calculated.

2.5. Cytotoxicity Assay

The cytotoxic effect of AuNRs on cancer cells was determined using a Cell Counting Kit-8 (CCK-8) assay (96992, Sigma-Aldrich). The cells were seeded in a 96-well plate (#3599, Corning) at 5 x 10^3 cells/well for CAL-27 and Hep G2, and at 4 x 10^3 for KYSE-30 and MCF-7 cells and incubated in a humidified incubator at 37 ℃ under 5% CO_2 for 24 hrs. Controls carried out were medium only, cells

Preprints (www.preprints.org) | NOT PEER-REVIEWED | Posted: 29 March 2021 doi:10.20944/preprints202103.0687.v1

only and uAuNRs only. After 24 hrs, serially diluted uAuNRs were added in 100 µl medium starting at a maximum concentration of 19 µg/ml (0.33 nM). After 72 hours incubation 10 µl of CCK-8 was added to each well and incubated for another 3 hrs at 37 ℃. Absorbance values of each well were read using a plate reader (#LB 940, Mithras, Berthold Technologies) at 450 nm wavelength.

2.6. Quantification of AuNR targeting

All four cancer cell lines were cultured in triplicate, on a 22 mm x 22 mm glass coverslips, as described previously. Biotinylated anti-EGFR monoclonal antibody was conjugated with AuNRs as described above[25][25][25][25][25][25][25](Busch et al., 2019)[25](25)(Busch et al., 2019)[25] [24-26]. After culturing the cells for 24 hr on coverslips, the supernatants were removed and either tAuNRs or uAuNRs in 2 ml fresh complete medium were added into each well. A total of 1 x 10^{11} (9.67 µg, 0.17 nM) uAuNRs or tAuNRs were added per well taking into account the average loss calculated (Fig.1) during the functionalisation process of the tAuNRs. Control wells received 2 ml complete medium only. After 18 hours incubation, the membranes of the cells were visualised using MemBrite dye kit according to the manufacturer's protocol (#30096T, Biotium, Fremont, USA) in a humidified incubator at 37 °C under 5% CO_2 for 5 minutes. After washing, the cells were fixed in 4% (v/v) PFA for 10 minutes at RT. After 5 washes with PBS, the coverslips were mounted onto glass slides using Prolong Gold antifade mountant containing DAPI (#P36930, ThermoFischer Scientific). These slides were left overnight at RT in a dry and dark place. Dark-field images were taken using an inverted microscope (Nikon Eclipse Tie, Nikon UK Limited) with a 100x oil-coupled objective. Dark-field, DAPI (nuclear stain) and Texas Red (membrane stain) channels were used to acquire 5 images per coverslip, per cancer cell line for each condition. Illumination and camera exposure levels were kept consistent between each modality for all cell lines imaged. ImageJ was used to quantify the level of optical scatter from AuNR populations. The image contrast tool was used in ImageJ to reduce the background signal from cell, enhancing the optical scatter from AuNRs. All groups had the same level of signal processing to enable comparisons between cell lines and targeted/untargeted AuNRs. The nuclear marker DAPI and membrane stains were used as a guide to quantify the number of AuNRs per cell. AuNRs were seen by darkfield microscopy as slightly orange-coloured small dots. The number of tAuNRs and uAuNRs per cell with clear and strong optical scattering intensity was counted and compared using a two-tailed non-parametric Mann-Whitney test for each cell line of all the four cancer cells following a One-way ANOVA analysis. The total number of samples used for each analysis was indicated and analysis was performed using GraphPad Prism 8 software.

3. Results

3.1. EGFR is highly expressed on HNSCC cell lines

Flow cytometry analysis showed that CAL-27 and KYSE-30 had an increased fluorescence intensity signal, as shown by the right shift of the histograms when stained for anti-EGFR antibody compared to that of isotype. No such shifts were observed for the EGFR negative cell lines Hep G2 and MCF-7 (Figure 2A). Overall, while 67.7% and 80.54% of the total cell counts were positive for anti-EGFR staining in KYSE-30 and CAL-27, respectively; only 5.7% and 2.3% were positive in Hep G2 and MCF-7 cells, respectively. The median fluorescent intensity (MFI) of EGFR expression also showed 8.7 and 7 fold increase for KYSE-30 and CAL-27 cells compared to isotype. The EGFR negative cell lines Hep G2 and MCF-7 had an MFI increase of 1.1 fold (Figure 2B). The % total count and MFI results imply a significantly increased EGFR expression level in KYSE-30 and CAL-27 compared to Hep G2 and MCF-7 cells. This was confirmed by immunofluorescent staining. This clearly demonstrated that the KYSE-30 and CAL-27 cancer cells bound the anti-EGFR antibody strongly compared to the Hep G2 and MCF-7 cancer cell lines (Figure 2C). While the KYSE-30 and CAL-27 showed a strong and specific extracellular membrane positivity for anti-EGFR antibody and there was no such reactivity measured in the Hep G2 and MCF-7 cancer cell lines.

Preprints (www.preprints.org) | NOT PEER-REVIEWED | Posted: 29 March 2021 doi:10.20944/preprints202103.0687.v1

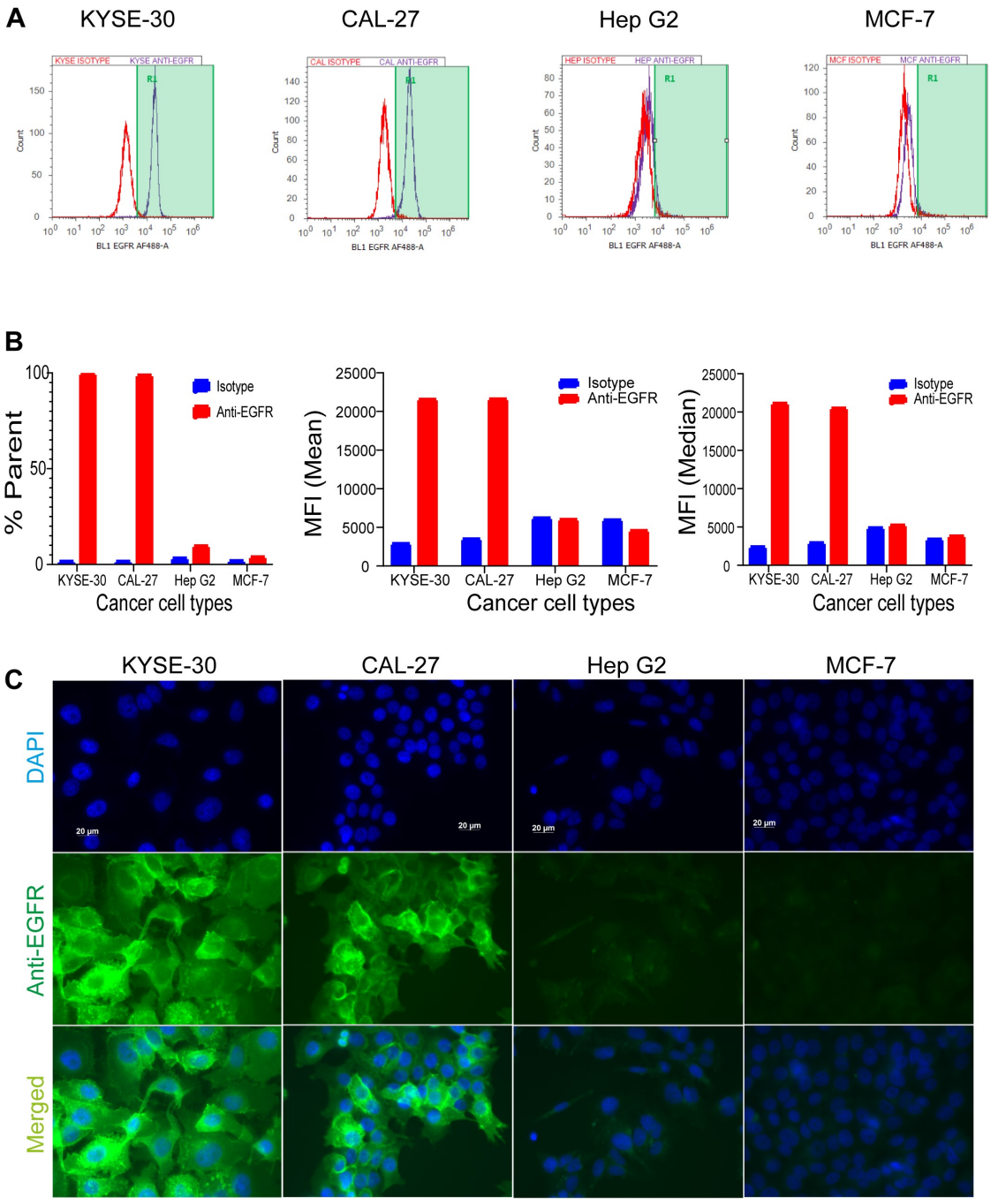

Figure 2. CAL-27 and KYSE-30 cancer cells express high level of EGFR. (**A**) Flow cytometry (red, isotype and blue, anti-EGFR staining); EGFR positive cancer cell lines KYSE-30 and CAL-27 had an 8.7 and 7-fold increase in fluorescence in the presence of anti-EGFR antibody, respectively while EGFR negative cancer cell lines Hep G2 and MCF-7 showed no such increase. The Y-axis represents the number of events (counts) and X-axis represents the fluorescence signal intensity from the EGFR-bound antibody. (**B**) Quantification of flow cytometry results as a % of total cells (% parent), mean and median fluorescence intensity of both isotype and anti-EGFR antibodies in 4 different cancer cell types. (**C**) Immunofluorescence staining of these four cancer cell lines using anti-EGFR and isotype antibodies showed a high expression of EGFR on KYSE-30 and CAL-27 compared to Hep G2 and MCF-7 cancer cell lines.

Preprints (www.preprints.org) | NOT PEER-REVIEWED | Posted: 29 March 2021 doi:10.20944/preprints202103.0687.v1

3.2. AuNRs show very low cytotoxicity even at high concentrations

uAuNRs showed very little toxicity to cancer cells even at the maximum concentration of 19 µg/ml used in this study. At this concentration, 72 ±8.3%, 79 ±4.3%, 67 ±12.2% and 101 ±8.2% of KYSE-30, CAL-27, Hep G2 and MCF-7 cancer cells were viable, respectively (Figure 3A-D). It was not possible to achieve a 50 % cell death with this maximum concentration dose of AuNRs and hence an IC_{50} for these particles was not obtained. Therefore, the 95% confidence interval (CI) was used to describe the AuNRs concentration required to cause 50% cell toxicity. Hence, based on these data the IC50 are therefore extrapolated to be over 100 µg/ml for each cell line.

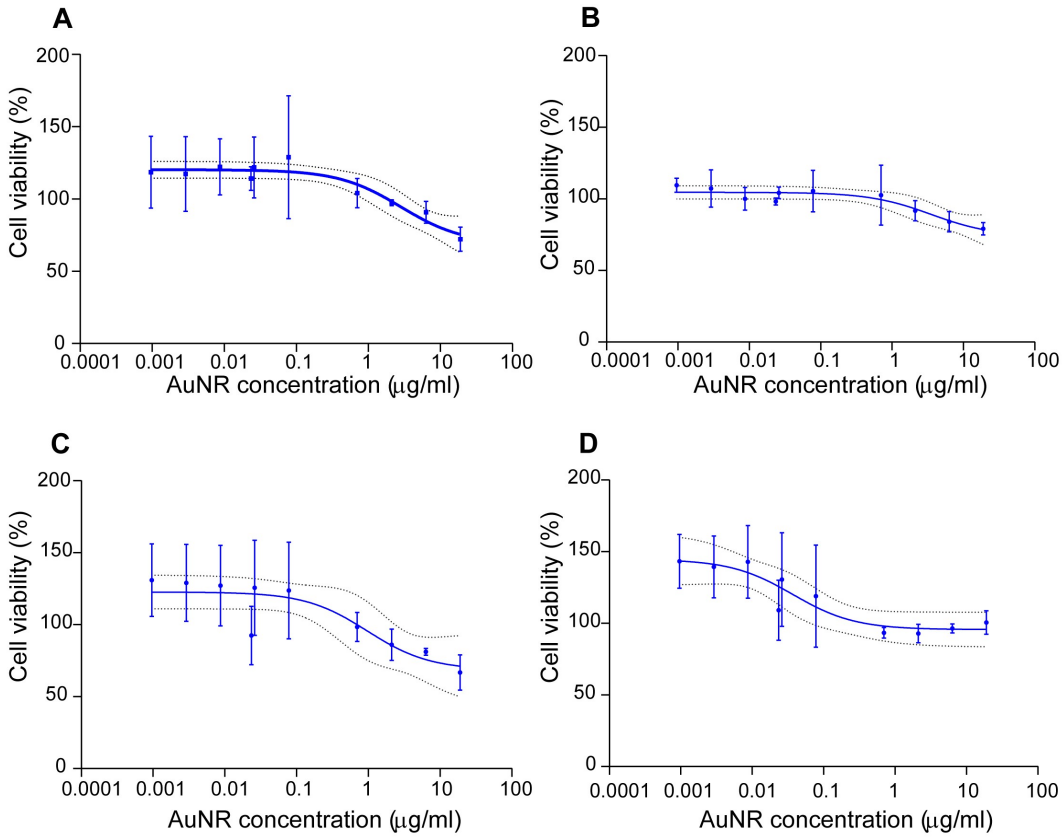

Figure 3. AuNRs had no cytotoxic effect on both EGFR positive and EGFR negative cancer cells. Dose-response curves for: (**A**) KYSE-30; (**B**) CAL-27; (**C**) Hep G2 and (**D**) MCF-7. N=3, the dotted lines represent 95% CI.

3.3. tAuNRs but not uAuNRs are increasingly associated with EGFR-positive cells

To identify if there was any differences in cellular tAuNRs uptake in EGFR positive KYSE-30 and CAL-27 cancer cells, the number of AuNRs associated with each cell following co-incubation was quantified based on small dots of clearly visible optical scatters from AuNRs. Dark-field images indicated a higher AuNRs optical scattering in targeted AuNR compared to untargeted AuNR (Figure 4A). A two-tailed nonparametric Mann Whitney t-test showed a significant difference ($p<0.0001$) between targeted and untargeted of KYSE-30, indicating that antibody functionalisation increased the number of tAuNRs per cell (Figure 5A). The same was observed for the second EGFR positive cancer cell line CAL-27 with a significantly higher ($p<0.0001$) number of AuNRs optical scatter per cell in the targeted compared to the untargeted AuNRs (Figure 5B).

Preprints (www.preprints.org) | NOT PEER-REVIEWED | Posted: 29 March 2021 doi:10.20944/preprints202103.0687.v1

When EGFR negative cancer cell lines, Hep G2 and MCF-7 were imaged under dark-field a low number of AuNRs was observed (Figure 4B).The number of AuNRs with optical scatter in Hep G2 cells indicated that there was a significantly higher ($p=0.006$) AuNRs per cell in the targeted group than in the untargeted group (Figure 5C). However, overall, this was insignificant compared to EGFR positive cancer cell lines, with a median of zero and four AuNRs per cell for untargeted and targeted groups, respectively. When the second EGFR negative cell line MCF-7 was analysed for the number of AuNRs per cell there was still a significantly higher ($p<0.0001$) number of AuNRs per cell in the targeted group compared to the untargeted group (Figure 5D). Again, the median number of AuNRs in MCF-7 remained low as in Hep G2 with zero and two AuNRs optical scatters per cell for untargeted and targeted groups, respectively.

Preprints (www.preprints.org) | NOT PEER-REVIEWED | Posted: 29 March 2021 doi:10.20944/preprints202103.0687.v1

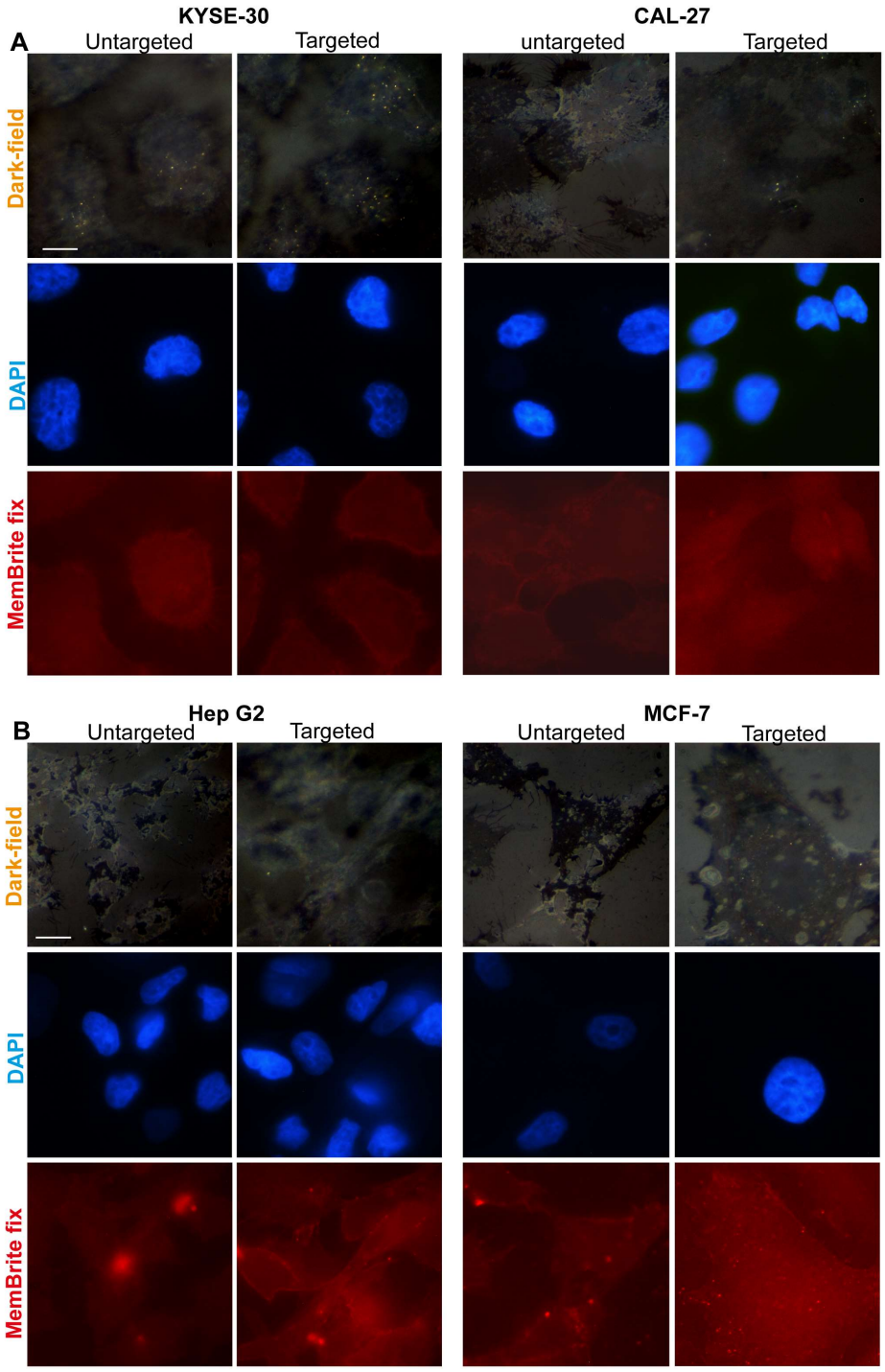

Figure 4. Images showing different intensity of AuNRs signal in EGFR positive and negative cancer cell lines. Dark-field, DAPI and Texas Red images of: (**A**) EGFR positive cancer cell line KYSE-30 and CAL-27 and (**B**) EGFR negative cancer cell lines Hep G2 and MCF-7 were taken for both tAuNRs and uAuNRs groups. All dark-field (where bright orange dots represent AuNRs), DAPI and Texas Red (MemBrite fix) images were captured using an inverted Nikon microscope with a uniform settings throughout. Scale bar, 100 µm.

Preprints (www.preprints.org) | NOT PEER-REVIEWED | Posted: 29 March 2021 doi:10.20944/preprints202103.0687.v1

There was a significantly higher ($p<0.0001$) number of tAuNRs in KYSE-30 compared to CAL-27, Hep G2 and MCF-7 showing that tAuNRs targeted KYSE-30 at an increasingly higher rate than the remaining three cancer cell lines (Fig. 5E). Likewise, there was a significantly higher ($p<0.0001$) number of tAuNRs per cell in CAL-27 compared to both Hep G2 and MCF-7 cancer cells. When the ratio of the median number of AuNRs in tAuNRs and uAuNRs were compared for each cell line and it was found to be 6.4, 9, 4 and 2 for KYSE-30, CAL-27, Hep G2 and MCF-7 cells, respectively. This indicates that while CAL-27 is a cancer cell line of choice over KYSE-30 for EGFR targeting experiment MCF-7 was found to be a good choice as EGFR negative control for EGFR targeting.

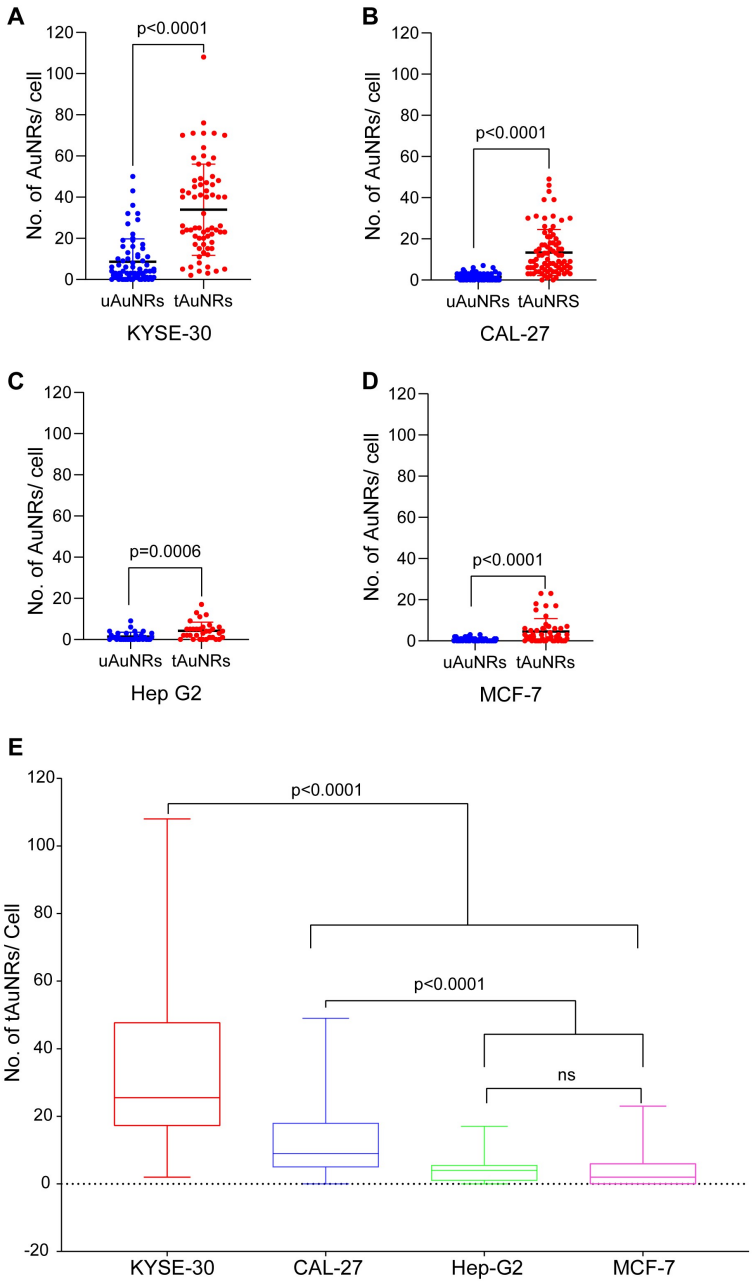

Figure 5. Targeting increased the number of AuNRs in cancer cells. A-E Plots show individual counts of AuNR imaged per cell with median and range shown. Mann-Whitney test showed that there was a significantly higher number of AuNRs counted in tAuNRs than in uAuNRs in: (**A**) KYSE-30 ($p<0.0001$); (**B**) CAL-27 ($p<0.0001$); (**C**) Hep G2 ($p=0.0006$) and (**D**) MCF-7 ($p<0.0001$). (**E**) Comparison of the

Preprints (www.preprints.org) | NOT PEER-REVIEWED | Posted: 29 March 2021 doi:10.20944/preprints202103.0687.v1

number of tAuNRs per cell show significantly increased number of tAuNRs in EGFR positive compared to EGFR negative cancer cell lines. The total number of cells counted were: KYSE-30 68 each for tAuNR and uAuNR; CAL-27 uAuNR, 68; tAuNR, 83; Hep G2 uAuNR and tAuNR, 33 each; and MCF uAuNR, 59 & tAuNR, 47.

Discussion

This *in vitro* study identified that anti-EGFR functionalisation increased the targeting potential of the AuNRs to EGFR expressing cell lines. Our findings in this study are supported by other studies including colorectal cancer [26], cervical cancer [27], skin cancer [28] and others where each of them found an increased uptake of functionalised gold nanoparticles in EGFR expressing cancer cells. In our study, although we used two cancer cell lines with an almost equal level of EGFR expression as shown by flow cytometry (Fig. 2), the number of tAuNRs detected in KYSE-30 were significantly greater ($p=0.002$) than those identified in CAL-27 cancer cells, although this seems to be due to an increased non-specific uptake of AuNRs. The reason as to such differences between these two cell lines of both polygonal shape and with more or less similar EGFR expression is not clear. However, examination of these cells under microscope, at 100x magnification, showed that KYSE-30 cells are much bigger and have more filopodia on their cell membrane than the CAL-27 cancer cells. To this end, it could be attributed to the differences in intracellular signalling cascade of these cells as the study of Khaznadar *et al* showed that despite both KYSE-30 and CAL-27 having comparable level of EGFR expression the level of EGFR phosphorylation in KYSE-30 was more than double that of CAL-27 cancer cells [29]. Phuc *et al* also found an increased efficiency of gold nanoparticles internalisation in A431 cells through clathrin-mediated endocytosis in the presence of EGF and the absence such ligands dramatically reduced the uptake of these nanoparticles [30]. The present findings of a significantly increased number of internalised tAuNRs in the EGFR positive cells compared to uAuNRs indicate the importance of targeting. However, the presence of a relatively higher number of tAuNRs than uAuNRs in EGFR negative cancer cells may be due to a change of surface charge on AuNRs following functionalisation which might affect their internalisation. The findings of more uAuNR in KYSE-30 compared to CAL-27 might contribute to differences in the physicochemical dynamics between these two cell lines following ligand-receptor binding.

Specific targeting of nanoparticles to improve therapy has long been a goal of many research groups and the results presented here are in accordance with EGFR-targeting for lung cancer and breast cancer. When the highly EGFR expressing lung cancer cell line, HCC87 and EGFR negative human kidney 293T cells were compared for uptake of peptide-conjugated triangular gold nanoplates, there was a significantly higher internalisation in the HCC87 than 293T cells [31]. When Li and colleagues compared the relative uptake of cetuximab functionalised gold nanoparticles (AuNPs) by EGFR expressing A431 and EGFR negative MDA-MB-453 cancer cells, using transmission electron microscopy (TEM), they found more AuNPs bound and accumulated in A431 cancer cells [28].

One of the probable obstacles with the use of nanoparticles in cancer therapy is their cell and tissue toxicity [32, 33]. Previous *in vitro* targeting studies reported effects of AuNR concentration, duration of incubation and surface functionalisation on viability of various cancer cell types. For example, Zhang *et al* reported minimal cytotoxic effect of AuNRs following incubation of MDA-MB-231 cells with 1.84 µg/ml of AuNRs for 24, 48 and 72 hrs, the presence of anti-EGFR or tAuNR showed some cytotoxic effect at 48 and 72 hr time points [34]. However, using A549 cancer cells Kao *et al* demonstrated lack of any of such differences in cell viability when such cells were incubated with either AuNPs-PEG or Cetuximab-AuNPs-PEG during the first 24 hr at a concentration of 0.625 µg/ml [35]. Still another study using MDA-MB-231 cells and different concentrations of anti-EGFR-Fucoidn-AuNRs at 24 and 48 hr time points also showed reduced cell toxicity effect of AuNRs even at a higher concentration of 100 µg/ml [36]. This is in agreement with our current findings where a maximum concentration of 19 µg/ml for 72 hr failed to produce any cell toxicity in all four cancer cell lines used in this study.

In conclusion, this study showed that the tAuNRs with a SPR at 1064 nm had an increased uptake in EGFR expressing cell lines compared to untargeted particles. However, the amount of uptake was dependant on the cell line, as it was significantly higher in the KYSE-30 compared to CAL-27 cancer cells. We hypothesise that the increased number of AuNRs in EGFR positive cancer cells is likely due to ligand-receptor binding activity [37] as opposed to simple passive diffusion mechanism or other forms of endocytosis. The work of Van Lehn *et al* showed increased internalisation of AuNPs into HeLa cells when incubated at 37 ℃ compared to 4 ℃, depending on their size and functionalisation [38], indicating the importance of active transport for the cell internalisation of nanoparticles. To the contrary, several older studies described enhanced permeability retention (EPR) effect [39, 40] as a mechanism of nanoparticles cell entry mechanism. However, a recent *in vivo* study [41] disputed this understanding of EPR effect, claiming that it is an active endocytosis (either inside vesicles or through transcellular channels) not passive diffusion which plays a major role in the nanoparticles cell entry mechanism. Overall, the result of this *in vitro* demonstration of targeting of particles with strong light absorbance in the second optical window, opens future potential for them to be used of molecular targeted light sensitisers for photoacoustic imaging and/or photothermal therapy applications.

Authors Contributions: Conceptualisation: T.E. and J.M.; methodology: T.E., N.I. and J.M.; software: T.E., N.I. and J.M.; validation: T.E.; formal analysis: T.E. and N.I.; investigation: T.E., J.M.; resources: J.M. and P.L.C.; data curation: T.E. and J.M.; writing – original draft preparation: T.E.; writing – review and editing: T.E., N.I., J.M. and P.L.C.; Visualisation: T.E., N.I. and J.M.; Supervision: J.M. and P.L.C.; funding acquisition: J.M. All authors have read and agreed to the published version of this manuscript.
Funding: This research project was funded by the Engineering and Physical Sciences Research Council (EP/S001069/1, EP/I000623/1 and EP/PO23266/1).
Acknowledgments: We thank Dr Hughes Research Group (LIMR, University of Leeds) for the donation of breast cancer cell line MCF-7.
Conflicts of Interest: The authors declare no conflict of interest. The funders had no role in the design of the study; in the collection, analyses, or Interpretation of data; in the writing of the manuscript, or in the decision to publish the results.

References

1. Debbage, P. and W. Jaschke, *Molecular imaging with nanoparticles: giant roles for dwarf actors.* Histochem Cell Biol, 2008. **130**(5): p. 845-75 DOI: 10.1007/s00418-008-0511-y.
2. Amendola, V., et al., *Surface plasmon resonance in gold nanoparticles: a review.* J Phys Condens Matter, 2017. **29**(20): p. 203002 DOI: 10.1088/1361-648X/aa60f3.
3. Guo, J., et al., *Gold nanoparticles enlighten the future of cancer theranostics.* Int J Nanomedicine, 2017. **12**: p. 6131-6152 DOI: 10.2147/IJN.S140772.
4. Roach, L., et al., *Morphological control of seedlessly-synthesized gold nanorods using binary surfactants.* Nanotechnology, 2018. **29**(13): p. 135601 DOI: 10.1088/1361-6528/aaa99d.
5. Chen, Y.S., et al., *Miniature gold nanorods for photoacoustic molecular imaging in the second near-infrared optical window.* Nat Nanotechnol, 2019. **14**(5): p. 465-472 DOI: 10.1038/s41565-019-0392-3.
6. Zhu, S., et al., *Near-Infrared-II (NIR-II) Bioimaging via Off-Peak NIR-I Fluorescence Emission.* Theranostics, 2018. **8**(15): p. 4141-4151 DOI: 10.7150/thno.27995.
7. Tao, Z., et al., *Early tumor detection afforded by in vivo imaging of near-infrared II fluorescence.* Biomaterials, 2017. **134**: p. 202-215 DOI: 10.1016/j.biomaterials.2017.04.046.
8. Zhao, J., D. Zhong, and S. Zhou, *NIR-I-to-NIR-II fluorescent nanomaterials for biomedical imaging and cancer therapy.* J Mater Chem B, 2018. **6**(3): p. 349-365 DOI: 10.1039/c7tb02573d.

9. Gargiulo, S., S. Albanese, and M. Mancini, *State-of-the-Art Preclinical Photoacoustic Imaging in Oncology: Recent Advances in Cancer Theranostics.* Contrast Media Mol Imaging, 2019. **2019**: p. 5080267 DOI: 10.1155/2019/5080267.
10. Aoki, H., et al., *Near-infrared absorbing polymer nano-particle as a sensitive contrast agent for photo-acoustic imaging.* Nanoscale, 2015. **7**(1): p. 337-43 DOI: 10.1039/c4nr04724a.
11. Zou, L., et al., *Current Approaches of Photothermal Therapy in Treating Cancer Metastasis with Nanotherapeutics.* Theranostics, 2016. **6**(6): p. 762-72 DOI: 10.7150/thno.14988.
12. Phan, T.T.V., et al., *Photoacoustic Imaging-Guided Photothermal Therapy with Tumor-Targeting HA-FeOOH@PPy Nanorods.* Sci Rep, 2018. **8**(1): p. 8809 DOI: 10.1038/s41598-018-27204-8.
13. Licitra, L., E. Felip, and E.G.W. Group, *Squamous cell carcinoma of the head and neck: ESMO clinical recommendations for diagnosis, treatment and follow-up.* Annals of Oncology, 2009. **20**(suppl_4): p. iv121-iv122.
14. Li, H., et al., *Genomic analysis of head and neck squamous cell carcinoma cell lines and human tumors: a rational approach to preclinical model selection.* Molecular Cancer Research, 2014. **12**(4): p. 571-582.
15. Grégoire, V., et al., *Squamous cell carcinoma of the head and neck: EHNS–ESMO–ESTRO Clinical Practice Guidelines for diagnosis, treatment and follow-up.* Annals of oncology, 2010. **21**(suppl_5): p. v184-v186.
16. Wise-Draper, T.M., et al., *Future directions and treatment strategies for head and neck squamous cell carcinomas.* Transl Res, 2012. **160**(3): p. 167-77 DOI: 10.1016/j.trsl.2012.02.002.
17. Bourhis, J., et al., *Phase III randomized trial of very accelerated radiation therapy compared with conventional radiation therapy in squamous cell head and neck cancer: a GORTEC trial.* J Clin Oncol, 2006. **24**(18): p. 2873-8 DOI: 10.1200/JCO.2006.08.057.
18. Gupta, T., et al., *Systematic review and meta-analyses of intensity-modulated radiation therapy versus conventional two-dimensional and/or or three-dimensional radiotherapy in curative-intent management of head and neck squamous cell carcinoma.* PLoS One, 2018. **13**(7): p. e0200137 DOI: 10.1371/journal.pone.0200137.
19. Savard, J., et al., *Cancer treatments and their side effects are associated with aggravation of insomnia: Results of a longitudinal study.* Cancer, 2015. **121**(10): p. 1703-11 DOI: 10.1002/cncr.29244.
20. Chung, C.H., et al., *Molecular classification of head and neck squamous cell carcinomas using patterns of gene expression.* Cancer cell, 2004. **5**(5): p. 489-500.
21. Walter, V., et al., *Molecular subtypes in head and neck cancer exhibit distinct patterns of chromosomal gain and loss of canonical cancer genes.* PloS one, 2013. **8**(2): p. e56823.
22. Upputuri, P.K. and M. Pramanik, *Photoacoustic imaging in the second near-infrared window: a review.* Journal of biomedical optics, 2019. **24**(4): p. 040901.
23. Mayerhofer, T.G., *Employing Theories Far beyond Their Limits - Linear Dichroism Theory.* Chemphyschem, 2018. **19**(17): p. 2123-2130 DOI: 10.1002/cphc.201800214.
24. Scarabelli, L., et al., *A "Tips and Tricks" Practical Guide to the Synthesis of Gold Nanorods.* J Phys Chem Lett, 2015. **6**(21): p. 4270-9 DOI: 10.1021/acs.jpclett.5b02123.
25. Busch, R.T., et al., *Optimization and Structural Stability of Gold Nanoparticle-Antibody Bioconjugates.* ACS Omega, 2019. **4**(12): p. 15269-15279 DOI: 10.1021/acsomega.9b02276.
26. Liszbinski, R.B., et al., *Anti-EGFR-Coated Gold Nanoparticles In Vitro Carry 5-Fluorouracil to Colorectal Cancer Cells.* Materials (Basel), 2020. **13**(2) DOI: 10.3390/ma13020375.
27. Liu, J., et al., *Anti-EGFR-Conjugated Hollow Gold Nanospheres Enhance Radiocytotoxic Targeting of Cervical Cancer at Megavoltage Radiation Energies.* Nanoscale Res Lett, 2015. **10**: p. 218 DOI: 10.1186/s11671-015-0923-2.
28. Li, S., et al., *Antibody-functionalized gold nanoparticles as tumor-targeting radiosensitizers for proton therapy.* Nanomedicine (Lond), 2019. **14**(3): p. 317-333 DOI: 10.2217/nnm-2018-0161.

29. Khaznadar, S.S., et al., *EGFR overexpression is not common in patients with head and neck cancer. Cell lines are not representative for the clinical situation in this indication.* Oncotarget, 2018. **9**(48): p. 28965-28975 DOI: 10.18632/oncotarget.25656.
30. Phuc, L.T.M. and A. Taniguchi, *Epidermal Growth Factor Enhances Cellular Uptake of Polystyrene Nanoparticles by Clathrin-Mediated Endocytosis.* Int J Mol Sci, 2017. **18**(6) DOI: 10.3390/ijms18061301.
31. Zhao, Y., et al., *Anti-EGFR Peptide-Conjugated Triangular Gold Nanoplates for Computed Tomography/Photoacoustic Imaging-Guided Photothermal Therapy of Non-Small Cell Lung Cancer.* ACS Appl Mater Interfaces, 2018. **10**(20): p. 16992-17003 DOI: 10.1021/acsami.7b19013.
32. Awasthi, R., et al., *Nanoparticles in Cancer Treatment: Opportunities and Obstacles.* Curr Drug Targets, 2018. **19**(14): p. 1696-1709 DOI: 10.2174/1389450119666180326122831.
33. Avalos, A., et al., *In vitro and in vivo genotoxicity assessment of gold nanoparticles of different sizes by comet and SMART assays.* Food Chem Toxicol, 2018. **120**: p. 81-88 DOI: 10.1016/j.fct.2018.06.061.
34. Zhang, M., et al., *Near-infrared photothermal therapy using anti-EGFR-gold nanorod conjugates for triple negative breast cancer.* Oncotarget, 2017. **8**(49): p. 86566.
35. Kao, H.-W., et al., *Evaluation of EGFR-targeted radioimmuno-gold-nanoparticles as a theranostic agent in a tumor animal model.* Bioorganic & medicinal chemistry letters, 2013. **23**(11): p. 3180-3185.
36. Manivasagan, P., et al., *Anti-EGFR antibody conjugation of fucoidan-coated gold nanorods as novel photothermal ablation agents for cancer therapy.* ACS applied materials & interfaces, 2017. **9**(17): p. 14633-14646.
37. Nair, S., et al., *Novel EGFR ectodomain mutations associated with ligand-independent activation and cetuximab resistance in head and neck cancer.* PLoS One, 2020. **15**(2): p. e0229077 DOI: 10.1371/journal.pone.0229077.
38. Van Lehn, R.C., et al., *Effect of particle diameter and surface composition on the spontaneous fusion of monolayer-protected gold nanoparticles with lipid bilayers.* Nano Lett, 2013. **13**(9): p. 4060-7 DOI: 10.1021/nl401365n.
39. Maeda, H., et al., *Tumor vascular permeability and the EPR effect in macromolecular therapeutics: a review.* J Control Release, 2000. **65**(1-2): p. 271-84 DOI: 10.1016/s0168-3659(99)00248-5.
40. Matsumura, Y. and H. Maeda, *A new concept for macromolecular therapeutics in cancer chemotherapy: mechanism of tumoritropic accumulation of proteins and the antitumor agent smancs.* Cancer Res, 1986. **46**(12 Pt 1): p. 6387-92.
41. Sindhwani, S., et al., *The entry of nanoparticles into solid tumours.* Nat Mater, 2020. **19**(5): p. 566-575 DOI: 10.1038/s41563-019-0566-2.